arXiv:2404.01865v1 [physics.plasm-ph] 2 Apr 2024

Attosecond gamma-ray flashes and electron-positron pairs in dyadic laser interaction with micro-wire

Prokopis Hadjisolomou[1,*], Tae Moon Jeong[1], Petr Valenta[1], Alexander J. Macleod[1], Rashid Shaisultanov[1], Christopher P. Ridgers[2], and Sergei V. Bulanov[1,3]

[1]ELI Beamlines Facility, Extreme Light Infrastructure ERIC, Za Radnicí 835, 25241 Dolní Břežany, Czech Republic
[2]York Plasma Institute, Department of Physics, University of York, Heslington, York, North Yorkshire YO10 5DD, UK
[3]National Institutes for Quantum Science and Technology (QST), Kansai Photon Science Institute, 8-1-7 Umemidai, Kizugawa, Kyoto 619-0215, Japan
[*]prokopis.hadjisolomou@eli-beams.eu

ABSTRACT

Beams of photons and charged particles of high energy and high brightness find application across a range of disciplines in both fundamental and applied sciences. The interaction of an ultra-intense laser with matter has been shown to be an efficient source of high-energy particles, but typical schemes generate spatially broad distributions with high-divergence and low-brightness. In this paper we report on emission of highly collimated, ultrabright, attosecond γ-photons and generation of dense electron-positron pairs via a tunable particle generation scheme which utilises the interaction of two high-power lasers with metallic micro-wire target. Irradiating the target with a radially polarised laser pulse first produces a series of high charge, short duration, electron bunches with low transverse momentum. These electron bunches subsequently collide with a counter-propagating high intensity laser. Depending on the intensity of the counter-propagating laser, the scheme can be used to generate either highly collimated ultra-bright MeV-GeV γ-beams or electron-positron bunches with densities approaching the solid density level.

High-energy photon and electron/positron beams have found important uses across a range of disciplines in modern science. A non-exhaustive list of their applications include radiotherapy[1,2], photonuclear fission[3–5], study of shockwaves[6,7], materials science[8–10], nuclear physics[11,12], neutron sources[13], astrophysical studies[14–17], study of fundamental physics[18–20] and positron generation[21–23]. Typically, generating high-energy particle beams requires large scale facilities and technology such as radio frequency accelerators. This can limit their availability for certain applications, motivating a growing interest in alternative sources.

The invention of the chirped pulse amplification technique[24] enabled the development of high power laser systems of pettawatt class, which have since become attractive candidates for particle production technologies[25–28]. Multi-petawatt laser facilities are now a reality with demonstration of the 10 PW level in ELI-NP[29,30], while a 10 PW laser system with an order of magnitude higher energy is soon expected at ELI-Beamlines[31]. Moreover, focusing the laser beam at a spot of 1.1 μm allowed surpassing the intensity level of 10^{23} Wcm^{-2} with a 4 PW laser[32]. The development of a 100 PW laser is ongoing[33,34], while the dual-beam 25 PW EPOPAL laser system[35,36] will allow more complex laser-target interaction setups.

The interaction of an ultra-intense laser ($\sim 10^{22}$ Wcm^{-2}) with matter results in the creation of energetic particle populations[37], namely electrons (e^-), positrons (e^+) and γ-photons. In particular, irradiating a solid density target with a high-power laser has been shown to be a particularly simple and efficient scheme for particle acceleration[38]. This results in a γ-ray flash[39], where high-energy γ-photons are emitted via multiphoton Compton scattering[38,40–45] , and the creation of high charge electron and positron beams via the multiphoton Breit-Wheeler pair-production[40,46,47]. While this scheme produces high particle yields and efficiently converts laser energy into total particle energy, some of the beam properties limit their usefulness for certain applications. In particular, when the high-power laser is linearly polarised both the γ-photons and electron-positron beams are emitted with large divergences, leading to low brightness.

In this paper we introduce a novel laser-matter interaction scheme for production of high-brightness strongly collimated γ-ray beams and/or high-charge and high-density bunches of e^-e^+ pairs which surpass the solid density level. The beams in each case appear in the form of a series of attosecond duration bunches with low-divergence. The proposed scheme is based on the interaction of two ultraintense lasers with a wire target. The overall process can be viewed as three step model, namely injection (first) , boosting (second) and collision (third) stage. Initially, a radially polarised (RP) laser[48] interacts with the wire target, ejecting localised electron bunches and accelerating them[49–51]. Once the electrons gain sufficient energy from the RP laser, a linearly polarised (LP) laser collides head-on with them yielding predominantly either a γ-ray flash or a large number of e^-e^+ pairs, depending on the focusing conditions of the LP laser.

Scheme Description

The staged interaction process is depicted in Fig. 1. At the injection stage (Fig. 1(a)), a RP laser focused by a parabola of f-number (the ratio of focal length to laser beam diameter) of 4 (f/4-RP laser) interacts with a micro-wire target. Alternative proposed schemes using two or more lasers are based on symmetric laser-target interaction scenarios[52–59]. Although interaction of strong lasers with micro/nano-thick wires has been previously studied[60–63], according to our knowledge none of these works employed RP mode, which is crucial for our scheme. The target is a cylinder of λ radius and 4λ length, where λ is the laser wavelength. The target density corresponds to a lithium micro-wire, at an electron number density of $n_e = 1.39 \times 10^{29}$ m^{-3}. Lithium, belonging in the alkali metals group, is the solid with lowest density, thus allowing easy penetration of the laser field in its volume; its skin depth has a relatively large value of $c/\omega_p \approx 14.3$ nm, where $\omega_p = \sqrt{n_e e^2/(\varepsilon_0 m_e)}$ is the plasma frequency, m_e is the electron mass, e is the elementary charge and ε_0 is the vacuum permittivity. The chosen target density is near-optimal for the 25 PW, 25 fs laser pulses used here. Lower density (foam) targets[64] cannot be used in the micro-wire target geometry due to localised density spikes, forbidding fabrication in the form of a micro-wire. Higher density targets allow lower field penetration in the target volume, resulting in less electron ejection after a threshold. Notably, wire targets are geometrically opposite to hollow cylindrical targets, extensively studied for attosecond electron bunches emission[65] and γ-photon emission[66,67]. Attosecond electron modulations are also observed in 'two-dimensional' wires[68,69].

In this work we used the three-dimensional (3D) EPOCH[70] particle-in-cell (PIC) code, as described in the Methods section. The RP laser field is imported into the simulation box at the edge of its Rayleigh range. Unlike LP lasers which focus to a central peak, RP lasers focus to a ring; with only exception being the λ^3 regime[71]. If the LP laser interacts with a wire of diameter larger than the focal spot diameter, then the electrons pile up near the target front surface forming a steep density gradient, in a similar way a flat-foil target interacts. On the other hand, if the wire dimensions are significantly smaller than the laser focal spot, then electrons are accelerated by the laser[72–75], but in the expense of volumetric reduction of the electron number, thus making the scheme not efficient. RP lasers bypass both of the aforementioned limitations, allowing laser acceleration of electrons in high density bunches. However, the wire radius should be small enough not to modify the propagation of the accelerating field; for the f/4-RP laser used, a target radius of λ is near-optimal. The wire length is also important, as a long wire results in reduced energy of the ejected electrons due to attractive Coulomb forces. For our simulation parameters, a wire of 4λ length is used, as it results in high ejected electron energy.

The simulation results are depicted in Fig. 2. Figs. 2(a-

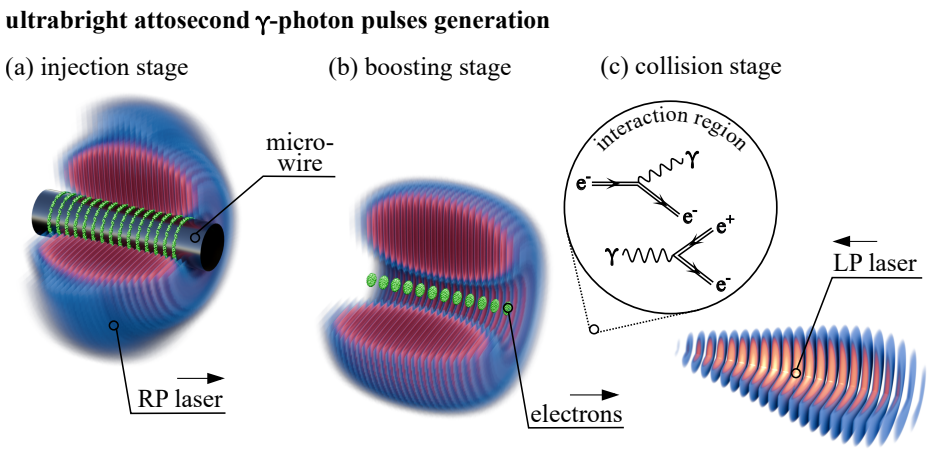

Figure 1. Illustrative interaction setup. **(a)** An f/4-RP laser interacts with a lithium wire target, resulting in axial electron emission. **(b)** The emitted electrons are accelerated up to the GeV energy level. **(c)** The emitted electrons collide with a counter-propagating LP laser. The laser-electron interaction results in a highly directional γ-ray flash accompanied by dense e^-e^+ pair generation.

c), 2(d-f) and 2(g-i) correspond to the injection, boosting and collision stages respectively, where the three stages are schematically illustrated in Fig. 1(a-c). The first figure column shows the laser intensity. For the injection and boosting stages, column two and three correspond to the electron mean kinetic energy and electron number density respectively. For the collision stage, the second column shows the generated positron mean energy and the third column shows the difference of electron to positron number densities.

Fig. 2(a-c) is at 50 fs simulation time, sufficient for the RP laser to interact with the micro-wire. Fig. 2(a) reveals that the laser field interacts with the wire target keeping it's propagation properties almost undisturbed, as the wire diameter is considerably smaller than the pulse diameter. Small field distortions are observed in the centre of the laser pulse due to electron bunching and acceleration. These electron bunches are dense enough for their emitted radiation to be observable on the laser intensity map.

In Fig. 2(b) the electron bunches correspond to a spectrum with a cut-off energy of ~ 0.6 GeV. Fig. 2(c) shows detachment of the electron bunches from the bulk target, moving along the laser propagation direction. The lower energy electrons are left in the target forming an exponential-like decaying distribution. The emitted electrons have a temporal distribution smaller than the laser duration, since a large portion of the emitted electrons are decelerated by emitted ions.

During the boosting stage, the laser accelerates the emitted electron bunches, as seen illustratively in Fig. 1(b) and quantitatively in Fig. 2(d-f) at 144 fs simulation time. At that time, the electron bunches contain ~ 2 % of the RP laser energy. The dashed line in Fig. 2 indicates the transition from the boosting to the collision stage. The RP laser is approximately at the focal spot, thus having flat wavefronts. The electron acceleration is quantified in Fig. 2(e), where the electron spectrum peaks at $\sim 0.2 \pm 0.1$ GeV. The rest of the spectrum is approximately flat, with a cut-off energy at ~ 2.2 GeV. The longitudinal momentum component of the bunches is two orders of magnitude higher than the transverse component, a necessary condition for collimated γ-photon emission.

The collision stage, illustrated in Fig. 1(c), introduces a LP ~ 25 PW 25 fs laser pulse, counter-propagating with respect to the electron bunches. The 0.8 μm wavelength LP laser is focused in spots of $0.8-20$ μm at FWHM. The laser peak intensity, I, range is $\sim 7\times10^{21}-4.4\times10^{24}$ Wcm^{-2}, corresponding to a dimensionless amplitude of $a_0 = eE/(m_e c\omega_l) \approx 57-1433$, where $E=\sqrt{2I/(\varepsilon_0 c)}$ is the peak electric field, ω_l is the central laser frequency and c is the speed of light in free space.

The laser-electron collision results in a bright γ-ray flash and/or a large number of e^-e^+ pairs, depending on the laser focusing conditions. The γ-photon emission and e^-e^+ pair generation ceases ~ 50 fs after the LP laser is introduced, with an emission time of ~ 13 fs at FWHM.

The field evolution at the end of the interaction, at 170 fs simulation time, is shown in Fig. 2(g). The field that corresponds to the RP laser keeps altering the momentum of the electron bunches even during the interaction with the LP laser, thus enhancing the overall γ-photon yield. This becomes evident by artificially removing the RP laser at the collision stage of the interaction, resulting in lower γ-photon yield.

One would naturally expect the generated e^-e^+ pairs to be emitted along the γ-photon emission direction. However, e^-e^+ pairs move opposite to the γ-photons, as they experience acceleration by the LP laser. The generated positrons have a Maxwell-Juttner distribution peaking at ~ 0.1 GeV and extending to ~ 2 GeV as shown in Fig. 2(h). The e^-e^+ pairs are located at symmetric sides within the laser field (Fig. 2(i)). Their density gradually decreases due to defocusing of the laser field, but maintaining a density above the den-

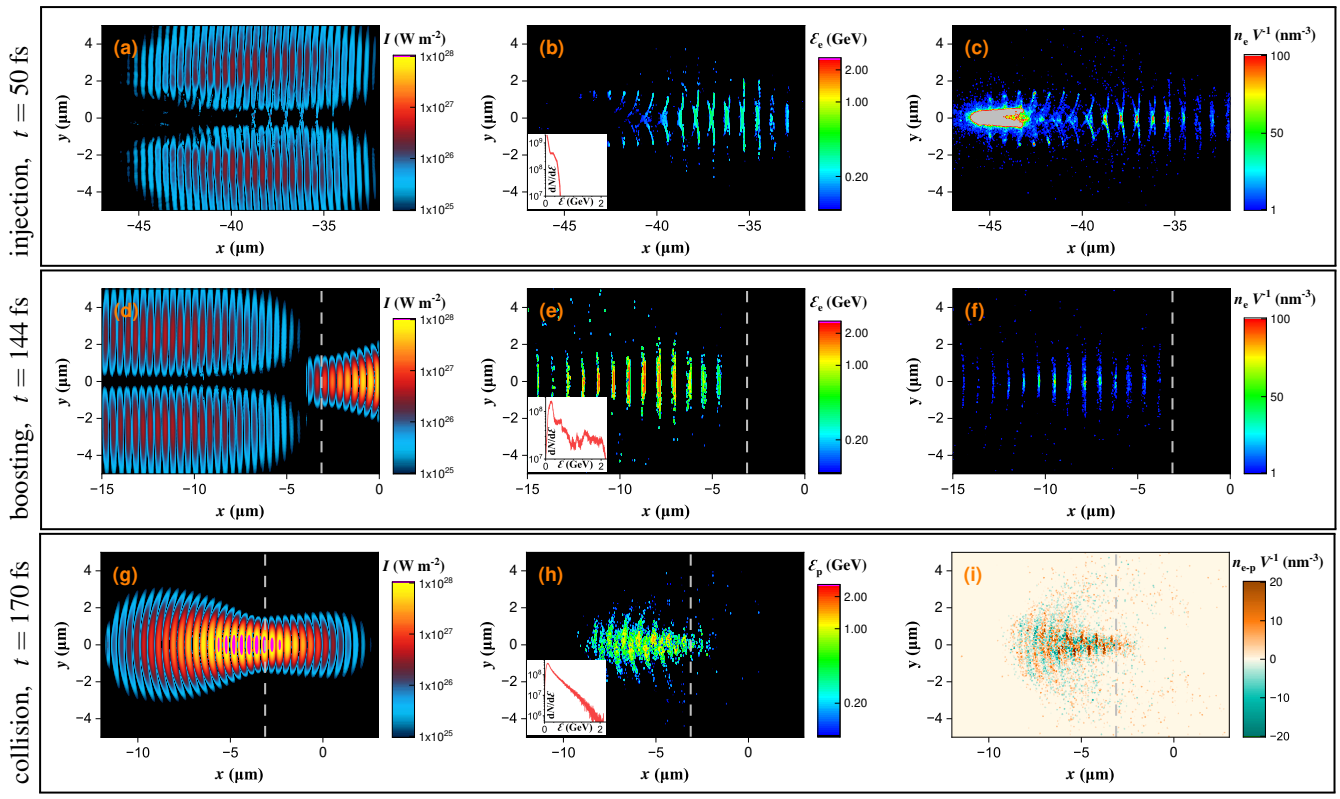

Figure 2. **(a)** Intensity, **(b)** electron mean kinetic energy and **(c)** electron number density, after the interaction of a f/4-RP laser with a lithium micro-wire. **(d)** Intensity, **(e)** electron mean kinetic energy and **(f)** electron number density, prior the interaction of collimated electron bunches (ejected from the micro-wire) with an f/1-LP counter-propagating laser. **(g)** Intensity, **(h)** positron mean kinetic energy and **(i)** electron minus positron number density, after the laser-electron interaction. For Figs. 2(b,e,h) the corresponding energy spectra are given as insets.

sity at FWHM (for each simulation case) for several tens of femtoseconds.

Attosecond Gamma-Flash and Dense e^-e^+ Pairs

During typical interactions of ultraintense lasers with matter, the emitter γ-photon spatial distribution has a double-lobe form with a divergence of $\sim 10^\circ$[64,76–79]. Although high laser to γ-photon energy conversion efficiency, κ_γ, has been predicted by employing multi-petawatt class lasers[76,79–84], the radiant intensity, I_Ω (giving a measure of the emitted γ-photon energy per unit time per unit solid angle), remains relatively low. One can increase I_Ω by reducing either the γ-photon emission time or the γ-photon divergence. Our proposed γ-ray flash scheme treats both aforementioned aspects simultaneously.

The radiant intensity of γ-photons shown in Fig. 3(a-d). Figs. 3(a,b) and Figs. 3(c,d) corresponds to the use of f/4-RP and f/2-RP lasers as an electron driver, respectively. Figs. 3(a,c) and Figs. 3(b,d) correspond to the use of f/20-LP and f/1-LP lasers as a counter-propagating laser, respectively. For relatively low a_0 values of the LP laser (Figs. 3(a,c)), a collimated γ-ray flash is obtained. The γ-photon beamlet is more collimated for the f/4-RP laser case, since the ratio of the transverse to the longitudinal momentum is lower compared to the f/2-RP laser case, although the latter gives higher electron energies. In the calculation of I_Ω we use a time interval of 1 fs (as explained later in the text). Thus, I_Ω exceeds 2700 PWsr^{-1} in Fig. 3(a), while it drops by a factor of ~ 5 in Fig. 3(c). The I_Ω versus a_0 is shown in Fig. 3(e), where the red colour represents the forward emitted γ-ray flash and the blue colour represents the backward emitted double-lobe γ-photon distribution. Another quantity describing the γ-ray source is the radiance, L_Ω, which is defined as I_Ω divided by the source size. In our case, γ-photons are emitted by the localised electron bunches, which can be approximated by a circle of radius of 473 nm. Thus, the radiance corresponding to Fig. 3(a) is $\sim 5.27 \times 10^{15}$ PWsr^{-1}m^{-2}. The highest known luminosity objects are the astrophysical γ-bursts. If we assume that a γ-ray burst luminosity is 10^{44} Js^{-1}[85] and it has a photoshpere diameter diameter of ~ 1000 km[86], then the radiance of our γ-source is approaching that of γ-ray bursts[87,88].

By decreasing the focal spot of the LP laser from 20 μm to 1 μm, then an $a_0 = 1146$ is reached, allowing prolific generation of e^-e^+ pairs. If one is interested predominantly on

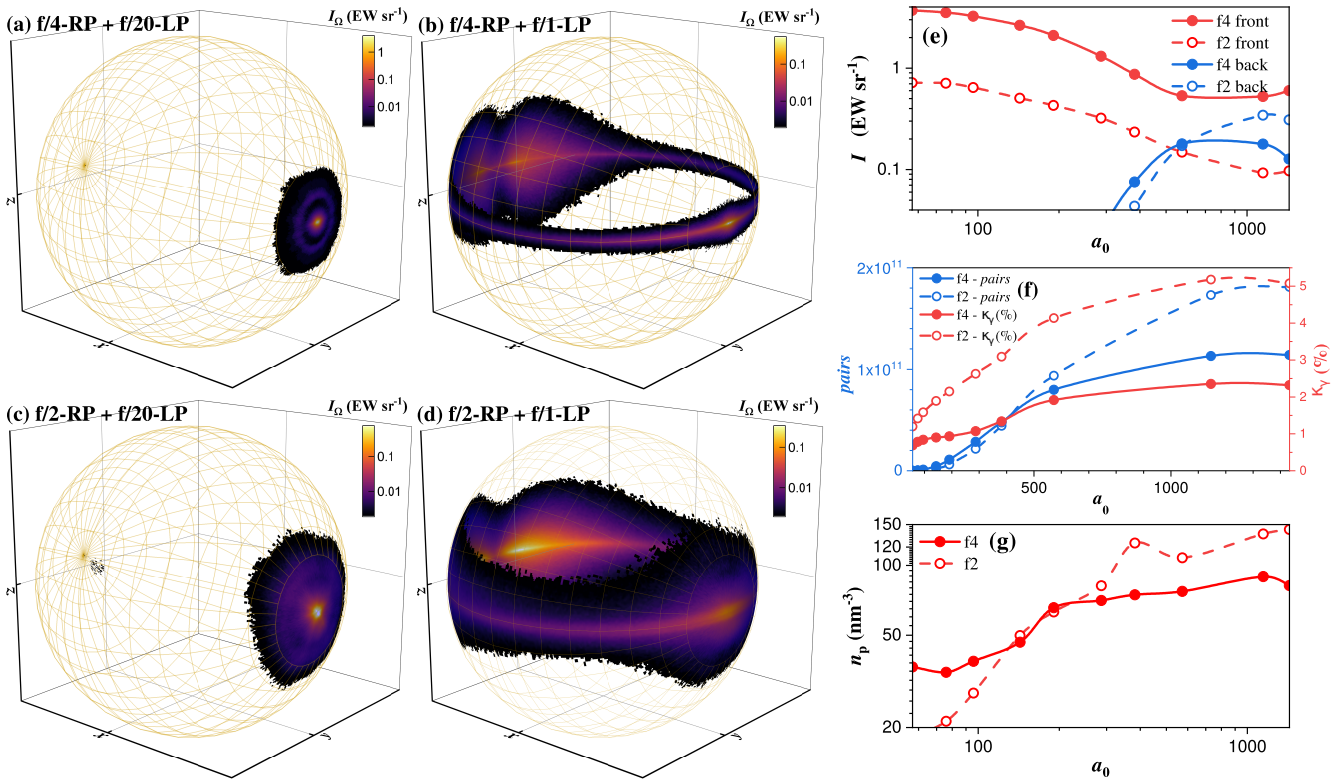

Figure 3. Radiant intensity corresponding to laser combination interaction scheme of **(a)** f/4-RP + f/20-LP **(b)** f/4-RP + f/1-LP **(c)** f/2-RP + f/20-LP **(d)** f/2-RP + f/1-LP lasers. In sub-figures 3(e-g) solid and dashed lines correspond to f/4-RP and f/2-RP lasers respectively. **(e)** The peak radiant intensity versus a_0 for the collimated γ-photon distribution (red) and for the double-lobe distribution (blue). **(f)** The left axis (blue) shows the number of e^-e^+ pairs produced and the right axis (red) shows κ_γ versus a_0. **(g)** The maximum electron density recorded in each simulation versus a_0.

e^-e^+ pair generation, then the f/2-RP laser case (injection and boosting stage) has a higher yield, since electrons reach higher energies. Approximately 1.8×10^{11} e^-e^+ pairs are generated by the LP laser with the electron bunches. The number of generated e^-e^+ pairs versus a_0 is shown in the left axis of Fig. 3(f), while the right axis shows κ_γ. The figure indicates an otherwise obvious conclusion, that the more γ-photons are emitted, the more e^-e^+ pairs are generated. Since those e^-e^+ pairs are generated in the small volume where the electron bunches are confined, their density value can exceed that of lithium, as seen in Fig. 3(g). The e^-e^+ pairs are driven by the LP laser in its propagation direction. Those backward moving fast electrons/positrons move in a strong laser field and emit secondary γ-photons with a double-lobe pattern. As seen in Fig. 3(e), I_Ω of the secondary emitted γ-photons can exceed that of the forward γ-photons. The forward γ-photon distribution decreases due to the e^-e^+ pair generation. We have proven that by reducing the focal spot of the LP laser from 20 μm to 4 μm and dropping the power of the RP laser from 25 PW to 1 PW, then the resulting γ-photon spectrum does not change significantly.

The small divergence on the γ-ray flash shown in Figs. 3(a,c) is better realised in Fig. 4. The sub-figures show projection of γ-photons on a plane orthogonal to the laser propagation axis, for energy intervals increasing by 0.25 GeV. The red circles correspond to divergence increments of 1°. The γ-photon counts are normalised to the peak value in each sub-figure.

The figure demonstrates a collimated γ-ray flash with a slightly elliptical profile. For notation, we assume an ellipse of major and minor axis corresponding to full-angle divergence defined as (a,b); the major axis coincides with the LP laser electric field oscillation direction. Here, $(a,b) \approx (1.95°, 1.45°)$ for the cumulative γ-photon signal, dominated by the relatively low (< 0.25 GeV) energy γ-photons. The γ-photon spatial distribution becomes more narrow for $0.5 - 0.75$ GeV, obtaining $(a,b) \approx (1.25°, 1°)$. For the f/20-LP + f/4-RP laser case, the γ-photon divergence increases to $\sim 4°$, with an asymmetric distribution.

For applications, one needs to know not only how intense the γ-ray flash is in a specific solid angle, but also information for the γ-photon energy. The aforementioned information are obtained through brilliance, as shown in Fig. 5(a) for the f/4-RP laser case and for various a_0 cases of the LP laser. The highest brilliance is achieved by a relatively weakly focused laser to a 20 μm diameter spot. The

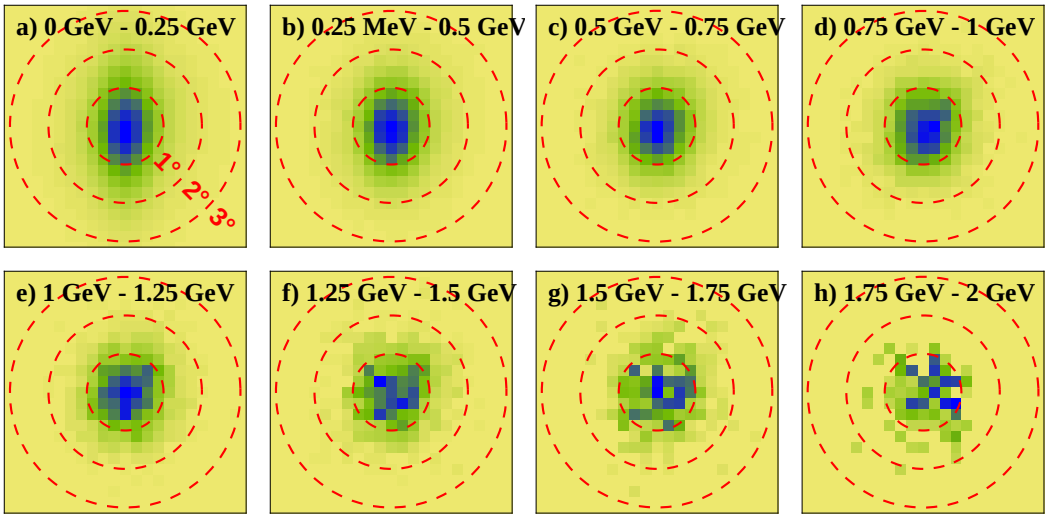

Figure 4. Normalised planar projection (on a plane 1 m far from the emitting source, the sub-figures has a width of 0.11 m) of the γ-photon distribution for the f/20-LP + f/4-RP laser case, in energy increments of 0.25 GeV.

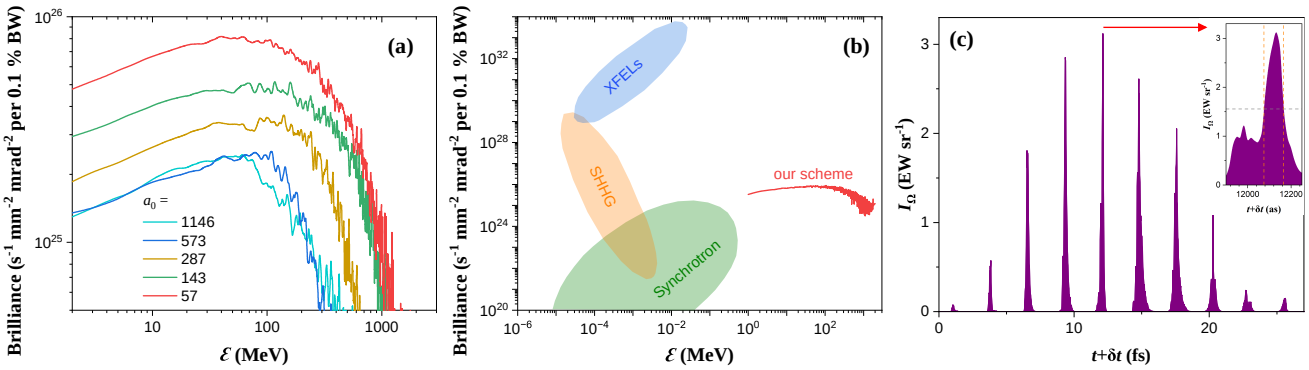

Figure 5. **(a)** Brilliance as a function of a_0, corresponding the f/20-LP + f/4-RP laser case. **(b)** Brilliance of x-ray sources from synchrotrons (green), SHHG (orange) and XFELs (blue) (data taken from[89]) compared to our scheme (red). **(c)** Temporal profile of the γ-ray flash, revealing a series of attosecond γ-photon pulses. The temporal axis employs an offset to shift the distribution at axis origin. The inset graph zooms at the γ-photon pulse at ~ 10 fs, indicated by the red arrow.

brilliance does not follow the typical exponentially decaying pattern which peaks for lower γ-photon energies[62,79,90–92], rather the peak distribution is at ~ 50 MeV. This peak value conveniently matches photonuclear reactions[93,94], which require tens of MeV energies. Our γ-photon source provides an extremely bright source in the multi-MeV range, reaching $\sim 9 \times 10^{25}$ s^{-1}mm^{-2} per 0.1% BW. In Fig. 5(b) we compare our γ-photon source with other schemes (see[89] and references therein), namely synchrotron, surface high-order harmonic generation (SHHG) and x-ray free electron lasers (XFELs). The proposed scheme generates high brilliance γ-photon pulses at energies which cannot be achieved by the aforementioned schemes.

Temporal analysis of the γ-ray flash for the peak brilliance case is shown in Fig. 5(c). The γ-photons are emitted in a series of attosecond pulses, with a period matching the laser frequency. The inlet figure zooms in the more intense of those pulses, having a duration of ~ 90 as at FWHM. Since the envelope of the γ-photon emission profile is ~ 13 fs at FWHM, the cumulative γ-photon emission time is approximately ~ 1 fs, as used above in I_Ω calculation. This is verified by Fig. 5(c) where the interval time is used, giving a similar value for the peak I_Ω compared to Fig. 3(a).

Conclusions

In this paper we introduce a novel dyadic laser-matter interaction scheme for emission of highly collimated, ultrabright, attosecond γ-ray flashes and generation of dense e^-e^+ pairs. Our interaction scheme employs a RP laser interacting with a micro-wire target, emitting localised electron bunches with longitudinal momentum component significantly higher than the transverse one. A counter-propagating LP laser interacts with the electron bunches, emitting a collimated γ-photon

beamlet. The divergence value is a function of the emitted γ-photon energy interval and it reaches values as low as $\sim 1^{\circ}$. Our scheme offers an ultrabright γ-photon source of $\sim 9\times10^{25}$ s^{-1}mm^{-2} per 0.1% BW at ~ 50 MeV. By controlling the LP laser focusing conditions we achieve prolific e^-e^+ pair generation, while at times of e^-e^+ pair peak generation rate, the positron density reaches a value that exceeds the solid density level.

Temporal analysis of the emitted γ-photon distribution reveals a series of ~ 100 as pulses, with a high radiant intensity of ~ 3 EWsr^{-1}. Compared with the pioneering work of Zewail, Mourou, L'Huillier, Agostini, and Krausz that has transformed chemistry using femtosecond and attosecond optical pulses (see[95,96] and references therein) and Hajdu and Chapman's invention using X-ray pulses, which brought the atomic view of materials[97–100], our invention of attosecond gamma-ray pulses can revolutionize photo-nuclear physics creating new era of science and technology.

Methods

The results of this work were obtained through use of the quantum electrodynamics[44,45,101] 3D EPOCH[70] PIC code. The Higuera-Cary[102] particle pusher is employed instead of the default Boris option, to obtain a more accurate trajectory of the relativistic electrons present in the simulation. The overall simulation results from two dependent simulations. In the first simulation we calculate the RP fields externally, and then import them into EPOCH, covering the left half of the simulation box. The laser pulse has a 0.8 μm wavelength, 25 fs pulse duration and it corresponds to a 25 PW laser. The laser is assumed to be focused by either f/2 or f/4 parabolas. The right half of the box contains no fields; there, a lithium cylinder is placed along the laser propagation axis, with radius of λ and length of 4λ. A moving window moving with the speed of light is used in the simulations, starting at 14.97 fs and stops at 27.35 fs for the f/2 case, while for the f/4 case the window starts at 4.23 fs and stops at 117.53 fs.

The initial and final time of the moving window are chosen in such a way that the simulation stops at a time of 2σ (where σ is the standard deviation of the pulse temporal profile) prior the electron bunches reach their highest energy. The field and particle data from the first simulation are imported into a second simulation, where a LP laser (same wavelength, temporal profile and power as the first laser) is launched from the right boundary of the simulation box, with a temporal offset of 2σ, focusing at a distance of $2\sigma c$ from the boundary. As a result, the peak intensity of the linearly polarised laser meets the electrons (the centre of their distribution) when they reach their peak energy value. The LP laser focal spot ranges from 0.8 μm to 20 μm. In all stages the simulation box has dimensions of 15.36 μm × 20.48 μm20.48 μm with a cell resolution of 5 nm × 40 nm40 nm.

Data availability

The data that support the findings of this study are available from the corresponding author, PH, upon reasonable request.

References

1. Weeks, K. J., Litvinenko, V. N. & Madey, J. M. The Compton backscattering process and radiotherapy. Med. Phys. **24**, 417–423, DOI: 10.1118/1.597903 (1997).
2. Papiez, L., DesRosiers, C. & Moskvin, V. Very high energy electrons (50 – 250 mev) and radiation therapy. Technol. Cancer Res. & Treat. **1**, 105–110, DOI: 10.1177/153303460200100202 (2002). PMID: 12622516, https://doi.org/10.1177/153303460200100202.
3. Cowan, T. E. et al. Photonuclear Fission from High Energy Electrons from Ultraintense Laser-Solid Interactions. Phys. Rev. Lett. **84**, 903–906, DOI: 10.1103/PhysRevLett.84.903 (2000).
4. Schwoerer, H. et al. Fission of actinides using a tabletop laser. Europhys. Lett. (EPL) **61**, 47–52, DOI: 10.1209/epl/i2003-00243-1 (2003).
5. Nedorezov, V. G., Turinge, A. A. & Shatunov, Y. M. Photonuclear experiments with Compton-backscattered gamma beams. Phys.-Uspekhi **47**, 341–358, DOI: 10.1070/pu2004v047n04abeh001743 (2004).
6. Ravasio, A. et al. Hard x-ray radiography for density measurement in shock compressed matter. Phys. Plasmas **15**, 060701, DOI: 10.1063/1.2928156 (2008).
7. Antonelli, L. et al. Laser-driven shock waves studied by x-ray radiography. Phys. Rev. E **95**, 063205, DOI: 10.1103/PhysRevE.95.063205 (2017).
8. Eliasson, B. & Liu, C. S. An electromagnetic gamma-ray free electron laser. J. Plasma Phys. **79**, 995–998, DOI: 10.1017/S0022377813000779 (2013).
9. Midgley, P. A. & Dunin-Borkowski, R. E. Electron tomography and holography in materials science. Nat. materials **8**, 271–280 (2009).
10. King, W. E. et al. Ultrafast electron microscopy in materials science, biology, and chemistry. J. Appl. Phys. **97**, 111101, DOI: 10.1063/1.1927699 (2005). https://pubs.aip.org/aip/jap/article-pdf/doi/10.1063/1.1927699/14936228/111101_1_online.pdf.
11. Tarbert, C. M. et al. Neutron Skin of ^{208}Pb from Coherent Pion Photoproduction, collaboration = Crystal Ball at MAMI and A2 Collaboration. Phys. Rev. Lett. **112**, 242502, DOI: 10.1103/PhysRevLett.112.242502 (2014).
12. Foris, B. & Papanicolas, C. N. Electron scattering and nuclear structure. Annu. Rev. Nucl. Part. Sci. **37**, 133–176 (1987).

13. Pomerantz, I. et al. Ultrashort Pulsed Neutron Source. Phys. Rev. Lett. **113**, 184801, DOI: 10.1103/PhysRevLett.113.184801 (2014).

14. Rees, M. J. & Mészáros, P. Relativistic fireballs: energy conversion and time-scales. Mon. Not. R. Astron. Soc. **258**, 41P–43P, DOI: 10.1093/mnras/258.1.41P (1992).

15. Bulanov, S. V. et al. On the problems of relativistic laboratory astrophysics and fundamental physics with super powerful lasers. Plasma Phys. Rep. **41**, 1–51, DOI: 10.1134/S1063780X15010018 (2015).

16. Philippov, A. A. & Spitkovsky, A. Ab-initio Pulsar Magnetosphere: Particle Acceleration in Oblique Rotators and High-energy Emission Modeling. Astrophys. J. **855**, 94, DOI: 10.3847/1538-4357/aaabbc (2018).

17. Takabe, H. & Kuramitsu, Y. Recent progress of laboratory astrophysics with intense lasers. High Power Laser Sci. Eng. **9**, e49, DOI: 10.1017/hpl.2021.35 (2021).

18. Telnov, V. Gamma-gamma, gamma-electron colliders (1998). hep-ex/9810019.

19. Tajima, T. & Homma, K. Fundamental Physics Explored with High Intensity Laser. Int. J. Mod. Phys. A **27**, 1230027, DOI: 10.1142/S0217751X1230027X (2012). 1209.2822.

20. Fedotov, A. et al. Advances in QED with intense background fields. Phys. Rep. **1010**, 1–138, DOI: https://doi.org/10.1016/j.physrep.2023.01.003 (2023). Advances in QED with intense background fields.

21. Gahn, C. et al. Generating positrons with femtosecond-laser pulses. Appl. Phys. Lett. **77**, 2662–2664, DOI: 10.1063/1.1319526 (2000).

22. Sarri, G. et al. Generation of neutral and high-density electron–positron pair plasmas in the laboratory. Nat. Commun. **6**, 6747, DOI: 10.1038/ncomms7747 (2015).

23. Kolenatý, D. et al. Electron-positron pairs and radioactive nuclei production by irradiation of high-Z target with γ-photon flash generated by an ultra-intense laser in the λ^3 regime. Phys. Rev. Res. **4**, 023124, DOI: 10.1103/PhysRevResearch.4.023124 (2022).

24. Strickland, D. & Mourou, G. Compression of amplified chirped optical pulses. Opt. Commun. **56**, 219–221, DOI: 10.1016/0030-4018(85)90120-8 (1985).

25. Bingham, R., Mendonca, J. & Shukla, P. Plasma based charged-particle accelerators. Plasma physics controlled fusion **46**, R1 (2003).

26. Malka, V. et al. Principles and applications of compact laser–plasma accelerators. Nat. physics **4**, 447–453 (2008).

27. Hooker, S. M. Developments in laser-driven plasma accelerators. Nat. Photonics **7**, 775–782 (2013).

28. Tajima, T. & Malka, V. Laser plasma accelerators. Plasma Phys. Control. Fusion **62**, 034004 (2020).

29. Tanaka, K. A. et al. Current status and highlights of the ELI-NP research program. Matter Radiat. at Extrem. **5**, 024402, DOI: 10.1063/1.5093535 (2020).

30. Radier, C. et al. 10 PW peak power femtosecond laser pulses at ELI-NP. High Power Laser Sci. Eng. **10**, e21, DOI: 10.1017/hpl.2022.11 (2022).

31. Danson, C. N. et al. Petawatt and exawatt class lasers worldwide. High Power Laser Sci. **7**, e54, DOI: 10.1017/hpl.2019.36 (2019).

32. Yoon, J. W. et al. Realization of laser intensity over $10^{23}\,W/cm^2$. Optica **8**, 630–635, DOI: 10.1364/OPTICA.420520 (2021).

33. Peng, Y. et al. Overview and status of station of extreme light toward 100 PW. Laser Rev. **49**, 97 (2021).

34. Li, Z., Kato, Y. & Kawanaka, J. Simulating an ultra-broadband concept for Exawatt-class lasers. Sci. Rep. **11**, DOI: 10.1038/s41598-020-80435-6 (2021).

35. Di Piazza, A., Willingale, L. & Zuegel, J. D. Multi-Petawatt Physics Prioritization (MP3) Workshop Report (2022). 2211.13187.

36. Zuegel, J. EP-OPAL - planning for a next-generation laser user facility dedicated to the study of ultra-high intensity laser-matter interactions (2023).

37. Mourou, G. A., Tajima, T. & Bulanov, S. V. Optics in the relativistic regime. Rev. Mod. Phys. **78**, 309–371, DOI: 10.1103/RevModPhys.78.309 (2006).

38. Gonoskov, A., Blackburn, T. G., Marklund, M. & Bulanov, S. S. Charged particle motion and radiation in strong electromagnetic fields. Rev. Mod. Phys. **94**, 045001, DOI: 10.1103/RevModPhys.94.045001 (2022).

39. Hadjisolomou, P. et al. Gamma-flash generation in multi-petawatt laser–matter interactions. Phys. Plasmas **30**, 093103, DOI: 10.1063/5.0158264 (2023).

40. Nikishov, A. I. & Ritus, V. I. QUANTUM PROCESSES IN THE FIELD OF A PLANE ELECTROMAGNETIC WAVE AND IN A CONSTANT FIELD. PART I. Sov. phys. JETP **19**, 529–541 (1964).

41. Brown, L. S. & Kibble, T. W. B. Interaction of Intense Laser Beams with Electrons. Phys. Rev. **133**, A705–A719, DOI: 10.1103/PhysRev.133.A705 (1964).

42. Goldman, I. I. Intensity effects in compton scattering. Phys. Lett. **8**, 103–106, DOI: https://doi.org/10.1016/0031-9163(64)90728-0 (1964).

43. Ritus, V. I. Quantum effects of the interaction of elementary particles with an intense electromagnetic field. J. Sov. Laser Res. **6**, 497–617, DOI: 10.1007/BF01120220 (1985).

44. Ridgers, C. P. et al. Dense Electron-Positron Plasmas and Ultraintense γ rays from Laser-Irradiated Solids. Phys. Rev. Lett. **108**, 165006, DOI: 10.1103/PhysRevLett.108.165006 (2012).

45. Ridgers, C. P. et al. Dense electron-positron plasmas and bursts of gamma-rays from laser-generated quantum electrodynamic plasmas. Phys. Plasmas **20**, 056701, DOI: 10.1063/1.4801513 (2013).

46. Reiss, H. R. Absorption of Light by Light. J. Math. Phys. **3**, 59–67, DOI: 10.1063/1.1703787 (1962).

47. Yakovlev, V. P. Electron-positron pair production by a strong electromagnetic wave in the field of a nucleus. Sov. Phys. JETP **22**, 223 (1966).

48. Jeong, T. M., Bulanov, S. V., Weber, S. & Korn, G. Analysis on the longitudinal field strength formed by tightly-focused radially-polarized femtosecond petawatt laser pulse. Opt. Express **26**, 33091–33107, DOI: 10.1364/OE.26.033091 (2018).

49. Varin, C. et al. Direct Electron Acceleration with Radially Polarized Laser Beams. Appl. Sci. **3**, 70–93, DOI: 10.3390/app3010070 (2013).

50. Powell, J. et al. Relativistic electrons from vacuum laser acceleration using tightly focused radially polarized beams (2024). 2402.08009.

51. Sun, T., Zhao, Q., Wan, F., Salamin, Y. I. & Li, J. X. Generation of Ultrabrilliant Polarized Attosecond Electron Bunches via Dual-Wake Injection. Phys. Rev. Lett. **132**, 045001, DOI: 10.1103/PhysRevLett.132.045001 (2024).

52. Luo, W. et al. Dense electron-positron plasmas and gamma-ray bursts generation by counter-propagating quantum electrodynamics-strong laser interaction with solid targets. Phys. Plasmas **22**, 063112, DOI: 10.1063/1.4923265 (2015).

53. Zhang, P., Ridgers, C. P. & Thomas, A. G. R. The effect of nonlinear quantum electrodynamics on relativistic transparency and laser absorption in ultra-relativistic plasmas. New J. Phys. **17**, 043051, DOI: 10.1088/1367-2630/17/4/043051 (2015).

54. Grismayer, T., Vranic, M., Martins, J. L., Fonseca, R. A. & Silva, L. O. Laser absorption via quantum electrodynamics cascades in counter propagating laser pulses. Phys. Plasmas **23**, 056706, DOI: 10.1063/1.4950841 (2016).

55. Vranic, M., Grismayer, T., Fonseca, R. A. & O-Silva, L. Electron–positron cascades in multiple-laser optical traps. Plasma Phys. Control. Fusion **59**, 014040, DOI: 10.1088/0741-3335/59/1/014040 (2016).

56. Gong, Z. et al. High-efficiency γ-ray flash generation via multiple-laser scattering in ponderomotive potential well. Phys. Rev. E **95**, 013210, DOI: 10.1103/PhysRevE.95.013210 (2017).

57. Drebot, I. et al. Matter from light-light scattering via Breit-Wheeler events produced by two interacting Compton sources. Phys. Rev. Accel. Beams **20**, 043402, DOI: 10.1103/PhysRevAccelBeams.20.043402 (2017).

58. Li, H. Z. et al. Ultra-bright γ-ray flashes and dense attosecond positron bunches from two counter-propagating laser pulses irradiating a micro-wire target. Opt. Express **25**, 21583–21593, DOI: 10.1364/OE.25.021583 (2017).

59. Yasen, N., Xie, B. & Liu, W. Dense positrons and γ-rays generation by lasers interacting with convex target. Plasma Sci. Technol. **23**, 015003, DOI: 10.1088/2058-6272/abcaed (2020).

60. Bargsten, C. et al. Energy penetration into arrays of aligned nanowires irradiated with relativistic intensities: Scaling to terabar pressures. Sci. Adv. **3**, e1601558, DOI: 10.1126/sciadv.1601558 (2017).

61. Li, H.-Z. et al. Ultra-bright γ-ray emission and dense positron production from two laser-driven colliding foils. Sci. Rep. **7**, 17312, DOI: 10.1038/s41598-017-17605-6 (2017).

62. Wang, W. M. et al. Collimated ultrabright gamma rays from electron wiggling along a petawatt laser-irradiated wire in the QED regime. Proc. Natl. Acad. Sci. **115**, 9911–9916, DOI: 10.1073/pnas.1809649115 (2018).

63. Zhang, L. et al. Brilliant attosecond γ-ray emission and high-yield positron production from intense laser-irradiated nano-micro array. Phys. Plasmas **28**, 023110, DOI: 10.1063/5.0030909 (2021).

64. Stark, D. J., Toncian, T. & Arefiev, A. V. Enhanced Multi-MeV Photon Emission by a Laser-Driven Electron Beam in a Self-Generated Magnetic Field. Phys. Rev. Lett. **116**, 185003, DOI: 10.1103/PhysRevLett.116.185003 (2016).

65. Naumova, N. et al. Attosecond Electron Bunches. Phys. Rev. Lett. **93**, 195003, DOI: 10.1103/PhysRevLett.93.195003 (2004).

66. Wang, T. et al. Power Scaling for Collimated γ-Ray Beams Generated by Structured Laser-Irradiated Targets and Its Application to Two-Photon Pair Production. Phys. Rev. Appl. **13**, 054024, DOI: 10.1103/PhysRevApplied.13.054024 (2020).

67. Rinderknecht, H. G. et al. Relativistically transparent magnetic filaments: scaling laws, initial results and prospects for strong-field QED studies. New J. Phys. **23**, 095009, DOI: 10.1088/1367-2630/ac22e7 (2021).

68. Ma, Y. Y. et al. Dense quasi-monoenergetic attosecond electron bunches from laser interaction with wire and slice targets. Phys. Plasmas **13**, 110702, DOI: 10.1063/1.2388958 (2006).

69. Shen, X., Pukhov, A. & Qiao, B. High-flux bright x-ray source from femtosecond laser-irradiated microtapes. Commun. Phys. **7**, 84, DOI: 10.1038/s42005-024-01575-z (2024).

70. Arber, T. D. et al. Contemporary particle-in-cell approach to laser-plasma modelling. Plasma Phys. Control. Fusion **57**, 113001, DOI: 10.1088/0741-3335/57/11/113001 (2015).

71. Mourou, G. et al. On the design of experiments for the study of relativistic nonlinear optics in the limit of single-cycle pulse duration and single-wavelength spot size. Plasma Phys. Rep. **28**, 12–27, DOI: 10.1134/1.1434292 (2002).

72. Wang, J. et al. Electron capture and violent acceleration by an extra-intense laser beam. Phys. Rev. E **58**, 6575–6577 (1998).

73. Zhu, L. J., Ho, Y. K., Wang, J. X. & Kong, Q. Violent acceleration of electrons by an ultra-intense pulsed laser beam. Phys. Lett. A **248**, 319 – 324 (1998).

74. Wang, P. X. et al. Vacuum electron acceleration by an intense laser. Appl. Phys. Lett. **78**, 2253–2255 (2001).

75. Braenzel, J. et al. Amplification of Relativistic Electron Bunches by Acceleration in Laser Fields. Phys. Rev. Lett. **118**, 014801 (2017).

76. Nakamura, T. et al. High-Power γ-Ray Flash Generation in Ultraintense Laser-Plasma Interactions. Phys. Rev. Lett. **108**, 195001, DOI: 10.1103/PhysRevLett.108.195001 (2012).

77. Vyskočil, J., Gelfer, E. & Klimo, O. Inverse Compton scattering from solid targets irradiated by ultrashort laser pulses in the 10^{22}˜10^{23} W/cm^2 regime. Plasma Phys. Control. Fusion **62**, 064002, DOI: 10.1088/1361-6587/ab83cb (2020).

78. Ji, L. L., Pukhov, A., Kostyukov, I. Y., Shen, B. F. & Akli, K. Radiation-Reaction Trapping of Electrons in Extreme Laser Fields. Phys. Rev. Lett. **112**, 145003, DOI: 10.1103/PhysRevLett.112.145003 (2014).

79. Hadjisolomou, P., Jeong, T. M. & Bulanov, S. V. Towards bright gamma-ray flash generation from tailored target irradiated by multi-petawatt laser. Sci. Rep. **12**, 17143, DOI: 10.1038/s41598-022-21352-8 (2022).

80. Lezhnin, K. V., Sasorov, P. V., Korn, G. & Bulanov, S. V. High power gamma flare generation in multi-petawatt laser interaction with tailored targets. Phys. Plasmas **25**, 123105, DOI: 10.1063/1.5062849 (2018).

81. Hadjisolomou, P., Jeong, T. M., Valenta, P., Korn, G. & Bulanov, S. V. Gamma-ray flash generation in irradiating a thin foil target by a single-cycle tightly focused extreme power laser pulse. Phys. Rev. E **104**, 015203, DOI: 10.1103/PhysRevE.104.015203 (2021).

82. Hadjisolomou, P. et al. Gamma-ray flash in the interaction of a tightly focused single-cycle ultra-intense laser pulse with a solid target. J. Plasma Phys. **88**, 905880104, DOI: 10.1017/S0022377821001318 (2022).

83. Hadjisolomou, P., Shaisultanov, R., Jeong, T. M., Valenta, P. & Bulanov, S. V. Effect of ultra-strong magnetic fields on laser-produced gamma-ray flashes. Phys. Rev. Res. **5**, 043153, DOI: 10.1103/PhysRevResearch.5.043153 (2023).

84. Shou, Y. et al. Brilliant femtosecond-laser-driven hard X-ray flashes from carbon nanotube plasma. Nat. Photon. **17**, 137–142, DOI: 10.1038/s41566-022-01114-8 (2023).

85. Piran, T. The physics of gamma-ray bursts. Rev. Mod. Phys. **76**, 1143–1210, DOI: 10.1103/RevModPhys.76.1143 (2005).

86. Wang, X. I. et al. GRB 210121A: A Typical Fireball Burst Detected by Two Small Missions. Astrophys. J. **922**, 237, DOI: 10.3847/1538-4357/ac29bd (2021).

87. Ruffini, R., Vereshchagin, G. & Xue, S. S. Electron–positron pairs in physics and astrophysics: From heavy nuclei to black holes. Phys. Rep. **487**, 1–140, DOI: https://doi.org/10.1016/j.physrep.2009.10.004 (2010).

88. Kumar, P. & Zhang, B. The physics of gamma-ray bursts & relativistic jets. Phys. Rep. **561**, 1–109, DOI: https://doi.org/10.1016/j.physrep.2014.09.008 (2015).

89. Jahn, O. et al. Towards intense isolated attosecond pulses from relativistic surface high harmonics. Optica **6**, 280–287, DOI: 10.1364/OPTICA.6.000280 (2019).

90. Zhu, X. L. et al. Dense GeV electron–positron pairs generated by lasers in near-critical-density plasmas. Nat. Commun. **7**, 13686, DOI: 10.1038/ncomms13686 (2016).

91. Zhu, X. L., Yu, T. P., Chen, M., Weng, S. M. & Sheng, Z. M. Generation of GeV positron and γ-photon beams with controllable angular momentum by intense lasers. New J. Phys. **20**, 083013, DOI: 10.1088/1367-2630/aad71a (2018).

92. Zhu, X. L. et al. Extremely brilliant GeV γ-rays from a two-stage laser-plasma accelerator. Sci. Adv. **6**, eaaz7240, DOI: 10.1126/sciadv.aaz7240 (2020).

93. Sun, X. Y. et al. Transmutation of long-lived fission products in an advanced nuclear energy system. Sci. Rep. **12**, 2240, DOI: 10.1038/s41598-022-06344-y (2022).

94. Deiev, O. S. et al. Photonuclear reactions cross-sections at energies up to 100 MeV for different experimental setups (2022). 2210.04324.

95. Mourou, G. A., Tajima, T. & B., S. V. Optics in the relativistic regime. Rev. Mod. Phys. **78**, 309–371, DOI: 10.1103/RevModPhys.78.309 (2006).

96. Krausz, F. & Ivanov, M. Attosecond physics. Rev. Mod. Phys. **81**, 163–234, DOI: 10.1103/RevModPhys.81.163 (2009).

97. Neutze, R., Wouts, R., van der Spoel, D., Weckert, E. & Hajdu, J. Potential for biomolecular imaging with femtosecond X-ray pulses. Nature **406**, 752–757, DOI: 10.1038/35021099 (2000).

98. Hajdu, J. The challenge offered by X-ray lasers. Nature **417**, 15–15, DOI: 10.1038/417015b (2002).

99. Chapman, H. N. et al. Femtosecond diffractive imaging with a soft-X-ray free-electron laser. Nat. Phys. **2**, 839–843, DOI: 10.1038/nphys461 (2006).

100. Chapman, H. N. et al. Femtosecond time-delay X-ray holography. Nature **448**, 676–679, DOI: 10.1038/nature06049 (2007).

101. Ridgers, C. P. et al. Modelling gamma-ray photon emission and pair production in high-intensity laser–matter interactions. J. Comput. Phys **260**, 273–285, DOI: 10.1016/j.jcp.2013.12.007 (2014).

102. Higuera, A. V. & Cary, J. R. Structure-preserving second-order integration of relativistic charged particle trajectories in electromagnetic fields. Phys. Plasmas **24**, 052104, DOI: 10.1063/1.4979989 (2017).

Acknowledgements

The authors thank Prof. Hajdu for useful discussion. The EPOCH code is in part funded by the UK EPSRC grants EP/G054950/1, EP/G056803/1, EP/G055165/1 and EP/M022463/1.

Author contributions

Author contributions: P.H., T.M.J. and S.V.B. conceived the work and participated in the interpretation of results; P.H. performed the PIC simulations and analysed the data;; P.H. and P.V. prepared the figures; R.S., A.J.M. and C.P.R. provided theoretical support for the results. The manuscript was written by all authors.

Competing interests

The authors declare no competing interests.